ACS APPLIED MATERIALS & INTERFACES
Research Article
www.acsami.org

Camera Method for Monitoring a Mechanochromic Luminescent β-Diketone Dye with Rapid Recovery

Tristan Butler, Alexander S. Mathew, Michal Sabat,[†,‡] and Cassandra L. Fraser*,[†]

[†]Department of Chemistry, University of Virginia, Charlottesville, Virginia 22904, United States
[‡]Department of Materials Science and Engineering, University of Virginia, 395 McCormick Road, Charlottesville, Virginia 22904, United States

Supporting Information

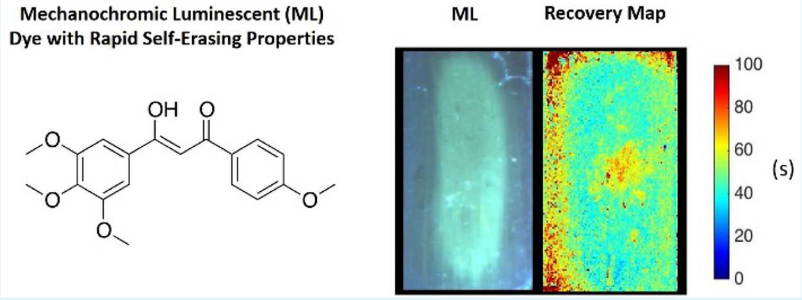

ABSTRACT: Mechanochromic luminescent (ML) materials, which show a change in emission due to an applied mechanical stimulus, are useful components in a variety of applications, including organic light-emitting diodes, force sensors, optical memory storage, and next-generation lighting materials. While there are many different ML active derivatives, few show room temperature self-erasing. Thin films of the methoxy substituted β-diketone, gbmOMe, initially exhibited blue (428 nm) emission; however, green (478 nm) emission was observed after smearing. The mechanically generated smeared state recovered so rapidly that characterization of its emission was difficult at room temperature using traditional luminescence techniques. Thus, a new complementary metal oxide semiconductor camera imaging method was developed and used to calculate the decay time of the mechanically generated smeared state (i.e., smeared-state decay; τ_{SM}) for gbmOMe thin films. Additionally, this method was used to evaluate substrate and film thickness effects on ML recovery for glass and weighing paper films. The recovery behavior of gbmOMe was largely substrate-independent for the indicated matrixes; however, thickness effects were observed. Thus, film thickness may be the main factor in determining ML recovery behavior and must be accounted for when comparing the recovery dynamics of different ML materials. Moreover, when heated above the melting point (T_m = 119 °C), bulk gbmOMe powders assumed a metastable state that eventually crystallized after a few minutes at room temperature. However, melted thin films remained in an amorphous state indefinitely despite annealing at different temperatures (50−110 °C). The amorphous phase was identified as a supercooled liquid via changing the rate of cooling in differential scanning calorimetry thermograms.

KEYWORDS: *mechanochromic luminescence, self-healing, camera RGB image analysis, supercooled liquids*

■ INTRODUCTION

Difluoroboron β-diketonate (BF_2bdk) materials are noted for their unique optical properties in both solution and the solid state.[1−3] Many BF_2bdk derivatives show room temperature phosphorescence (RTP) in poly(lactic acid) (PLA) matrixes and can be used to quantify oxygen in biological systems.[4−6] Additionally, BF_2bdk materials exhibit mechanochromic luminescence (ML) with spontaneous recovery[7] as well as aggregation induced emission[8] (AIE) and solvatochromism.[9] These diverse properties coupled with their straightforward synthesis make this family of boron dyes potentially useful for numerous applications such as mechanical sensors, next-generation light sources, display technologies, security inks, and biological probes.[10−16] Similar to their boronated counterparts, unique solution and solid-state optical properties have also been observed in boron-free β-diketone (bdk) materials.[17] The methoxy-substituted dinaphthoylmethane derivative (dnmOMe) showed solvatochromism and AIE in addition to high contrast ML with rapid spontaneous recovery.[18] Furthermore, because β-diketones, including methoxy-substituted derivatives, show large molar absorptivities and photostabilities, they have been screened and used as UV absorbing additives in sunscreens.[19]

Successful integration of bdk dyes into commercial applications requires a thorough understanding of structure−property relationships and material processing parameters (e.g., temperature, thickness, and substrate). Prior reports describe the effects of alkyl chain length,[7,20] halide substitution,[21] arene

Received: February 10, 2017
Accepted: April 17, 2017

DOI: 10.1021/acsami.7b01985

size,[22] and even BF_2 coordination on the optical and room temperature self-healing properties of ML materials.[18] Substitution of stimuli responsive materials with different donor and acceptor groups is also an common strategy for modulating solid-state ML properties such as emission wavelength, intensity, and spontaneous recovery.[23−26] For example, alkoxy substitution modulates solution and solid-state optical properties through electronic properties and control of molecular packing.[27−30] Recently, Sket et al., showed that the ML active, methoxy-substituted BF_2bdk 1-phenyl-3-(3,5-dimethoxyphenyl)-propane-1,3-dione can be crystallized as uniquely emissive polymorphs whose formation is partially governed by the different conformations of the methoxy substituents.[31] Additionally, selective methoxy-substitution can induce intramolecular charge transfer (ICT) in certain bdk dyes, which has been correlated with the solvatochromic and phosphorescent properties.[18,32] Literature precedent combined with the abundance and variety of commercially available starting materials makes methoxy substitution a good strategy for tuning the optical and ML properties of bdk materials. Thus, in this study, we employed methoxy substitution to modulate the emission and self-recovery properties of a bdk dye. Though the tetramethoxy-substituted dibenzoylmethane, 3-hydroxy-3-(4-methoxyphenyl)-1-(3,4,5-trimethoxyphenyl)prop-2-en-1-one (gbmOMe) was synthesized and evaluated previously as a sunscreen additive,[19] the stimuli responsive solid-state properties of gbmOMe have yet to be reported.

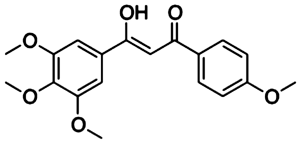

gbmOMe

Material processing parameters such as temperature, dye−substrate interactions, film thickness, and repeated smearing also influence ML properties. The thermal properties of luminophores are important both for fabrication and because the mechanically triggered changes in optical properties are often the result of temperature-dependent crystalline-to-amorphous phase transitions.[21,33] For example, amorphous melt quenched thiophene and furan substituted BF_2bdk derivatives showed red-shifted emission compared to their emission in the crystalline state.[34] Thus, it is possible to access the amorphous phase of these materials via thermal or mechanical stimulation. Similar optical properties were observed for a triphenyl amine (TPA)-based material reported by Mizuguchi et al., which showed rapid ML recovery of a green-yellow emissive state that was produced via melting and cooling to room temperature in addition to smearing.[35] The identity of this emissive melted state was determined to be a supercooled liquid with red-shifted emission resulting from a twisted intramolecular charge transfer (TICT) state. Additionally, Kim et al. observed a high contrast change in emission for an alkylated diketopyrrolopyrrole due to shear-triggered crystallization of a thermally stable supercooled liquid state.[36] The phase transition was attributed to a small Gibbs free energy difference between the crystalline and the supercooled liquid state. Such changes in emission were even activated by small forces associated with live cell attachment. This example demonstrates an application for thermally stable amorphous solids, namely, as cell force sensors. Yet, despite their potential for optical and optoelectronic uses[37,38] and for improving the solubility of various active pharmaceutical ingredients and excipients,[39] supercooled liquids are relatively rare.

Compared to temperature, relatively little is known about how film thickness, dye−substrate interactions, and repeated smearing affect ML recovery properties. This may be due in part to the relative scarcity of RT self-healing systems. Furthermore, certain fast recovering ML dyes such as diketones are incompatible with standard room temperature fluorimetry, given they recover faster (seconds to minutes) than the time required to record a spectrum. On the other hand, slow self-erasing ML systems are inconvenient to monitor given intensity changes little over long time periods, and subtle substrate and film thickness effects could be imperceptible. Additionally, standard characterization often averages emission intensity over relatively large sample regions and does not account for localized differences in ML recovery. Alternatively, techniques that excite locally do not provide good spatial resolution of ML recovery processes. To address some of these challenges and obtain 2D spatiotemporal information on ML recovery as a function of substrate, thickness, and smearing, we developed a video camera method to monitor the intensity decay of individual pixels over time. Previously, we employed this camera imaging technology to track photostability, oxygen-dependent lifetime,[40] and intensity[6] of BF_2bdkPLA phosphorescent materials. This method not only allows for investigation of recovery dynamics of gbmOMe thin films averaged as a whole but also provides a spatially resolved means of evaluating localized recovery effects associated with the smearing process. Structural and stimuli responsive properties of gbmOMe were also investigated using powder and single crystal X-ray diffraction, differential scanning calorimetry (DSC), and through excitation and emission spectra recorded at room temperature and 77 K.

■ EXPERIMENTAL DETAILS

Materials. Solvents THF and CH_2Cl_2 were dried over molecular sieves activated at 300 °C as previously described.[41] Reactions were monitored using silica TLC plates. Compounds purchased from Sigma-Aldrich were reagent grade and used without further purification. The β-diketone 3-hydroxy-3-(4-methoxyphenyl)-1-(3,4,5-trimethoxyphenyl)prop-2-en-1-one (gbmOMe) was synthesized as previously described.[2]

Methods. ^{1}H NMR (600 MHz) spectra were recorded in dilute $CDCl_3$ using a Varian VRMS/600. Spectra were referenced to the signals for residual protio-$CDCl_3$ at 7.26 ppm and coupling constants were recorded in Hz. UV−vis spectra were collected on a Hewlett-Packard 8452A diode-array spectrophotometer. Steady-state fluorescence emission and excitation spectra were obtained on a Horiba Fluorolog-3 Model FL3-22 spectrofluorometer (double-grating excitation and double-grating emission monochromator). Time-correlated single-photon counting (TCSPC) fluorescence lifetime measurements were performed with a NanoLED-370 (λ_{ex} = 369 nm) excitation source and a DataStation Hub as the SPC controller. Lifetime data were analyzed with DataStation v2.4 software from Horiba Jobin Yvon. Solid-state quantum yield measurements were acquired using a F-3029 Quanta-Φ Integrating Sphere purchased from Horiba Scientific and analyzed using FluorEssence software. Fluorescence quantum yields, φ_F, in CH_2Cl_2 were calculated versus a dilute quinine sulfate solution in 0.1 M H_2SO_4 as a standard using a previously described method[42] and the following values: φ_F quinine sulfate in 0.1 M sulfuric acid = 0.54;[43] n_D[44] 0.1 M H_2SO_4 = 1.33; n_D[45] CH_2Cl_2 = 1.424. Optically dilute CH_2Cl_2 solutions of all samples were prepared in 1 cm path length quartz cuvettes with absorbances <0.1 (au). ML emission was observed by applying a constant, gentle pressure via a cotton swab or a Kimwipe against glass and weigh paper films. Powder XRD patterns were obtained using a Panalytical X'Pert

Pro MPD diffractometer operating at 40 kV and 40ma using Cu Kα radiation. DSC was performed on the pristine powders using a TA Instruments DSC 2920 Modulated DSC, and data were analyzed using the Universal Analysis software v2.3 from TA Instruments. Thermograms were recorded using the standard mode while heating at a constant rate of 10 °C/min. The cooling rate was changed as indicated for different measurements but was held constant throughout a given heating/cooling cycle.

Crystallographic Information. Crystals for single crystal XRD were grown by vapor diffusion of hexanes into ethyl acetate. Data collection was performed using a Bruker Kappa Duo CCD diffractometer at −120 °C with Mo Kα radiation. Crystal data for gbmOMe: orthorhombic space group *Pbca*; a = 17.7840(19); b = 7.5472(8); c = 7.5472(8) Å; β = 90°, Z = 8, V = 3393.2(6) Å^3. The structure was solved by the charge flipping method of the Bruker SHELXTL program and refined to an R = 0.0475 using 5976 reflections with $I > 2\sigma(I)$.

Preparation of Thin Films. Bulk powder films for ML characterization were fabricated on weigh paper substrates by smearing ~2 mg of sample across the entire surface with a Kimwipe. Drop cast films were prepared by adding 20 drops of gbmOMe/THF solutions (0.090 and 0.018 M) to 3″ × 1″ weigh paper and glass microscope slides. Spin-cast films were made using a Laurel Technologies WS-65OS spin-coater and applying 20 drops to glass microscope slides rotating at 3000 rpm. Both spin-cast and drop cast samples were dried under vacuum for 20 min prior to annealing at 75 °C for 10 min. Green emission remained after annealing, so films were gently smeared with a Kimwipe followed by annealing at 75 °C for another 10 min to produce uniform blue emission.

Smeared State Decay Measurements. Spontaneous smeared emission decay measurements were performed at room temperature using a PGR GS3-U3-41C6C-C video camera with a complementary metal oxide semiconductor chip capable of 90 frames per second (FPS) at a maximum resolution of 2048 × 2048 pixels. The camera was also equipped with a Spacecom f/0.95 50 mm lens and an Edmund Optics 425 nm long pass filter to minimize excitation background. The camera was operated with a Lenovo W530 laptop connected via a USB 3.0 cable. Point Gray FlyCap2 software was used to record videos of smeared glass and weigh paper films, and the data were analyzed using a custom MATLAB 2014b program. The camera was placed approximately 0.5 m above the sample, which was illuminated with a 100W Black-Ray B-100AP/R lamp at 365 nm located ~10 cm above the sample. Videos of recovering samples were recorded using a frame rate of 1 frame per second (fps), and the intensity of the green channel was monitored over time. The initial intensity of the green channel due to sample emission prior to smearing was subtracted from each pixel before fitting data to a double exponential decay, and the pre-exponential weighted lifetime was reported. Photostability measurements were performed using the same experimental setup as recovery measurements and irradiating the sample continuously for 4 h while monitoring the pixel intensity every 5 min.

■ RESULTS AND DISCUSSION

Optical Properties in Solution. The β-diketone gbmOMe was synthesized via Claisen condensation of ester and ketone building blocks as previously described.[2] The optical properties of gbmOMe were measured in dichloromethane solution (Figure S1, Table S1). UV−vis spectra reveal an absorption peak (λ_{abs}) at 365 nm with a molar absorptivity of 64 000 M^{-1} cm^{-1}. Though the solution appeared nonemissive to the eye due to a very low quantum yield (Φ = 0.01%), a peak was detectable at λ_{em} = 427 nm in the steady-state emission spectrum.

Solid State Thermal Properties. To achieve high color contrast, mechanochromic luminescent materials are typically processed by thermal annealing to produce an ordered emissive state. Smearing then generates a red-shifted amorphous state. However, qualitative screening of the thermal properties of gbmOMe not only revealed differences between bulk solid and thin film samples but also showed new phenomena. As a bulk powder, gbmOMe glowed light blue (λ_{em} = 453 nm, Φ = 5.1%) under UV irradiation. When the powder was heated above the melting point, a melted (MT) viscous green emissive phase formed (λ_{MT} = 481 nm, Φ = 10.0%). Crystallization of this melted phase occurred within a few minutes after the heat source was removed to yield a blue-emissive solid. However, similar crystallization was not observed for melted thin films of gbmOMe. Instead, the green emissive state persisted upon cooling. Powder XRD patterns further confirmed that bulk gbmOMe is crystalline and MT thin films are amorphous, as no peaks were observed in the diffraction pattern for the latter samples (Figure S2). This relative difference in thermal stability of the MT phase for bulk powder and thin films may indicate a thickness dependence on the crystallization rate of melted gbmOMe.

The thermal properties of gbmOMe were further investigated using differential scanning calorimetry. The sample was heated at a constant rate of 10 °C/min while the rate of cooling was varied for each cycle (Figure 1). Each cycle was performed in succession to probe the thermal history. Thermograms show that gbmOMe melts at 119 °C regardless of cooling rate. When cooled faster than 1 °C/min, crystallization was not observed for the duration of the cooling cycle; however, crystallization was observed upon subsequent heating. When the rate was slow enough (1 or 0.5 °C/min), crystallization could be seen during the cooling cycle. These results indicate that the difference in thermal stability of the green amorphous state of gbmOMe as a bulk melt compared to melted thin films could be due to

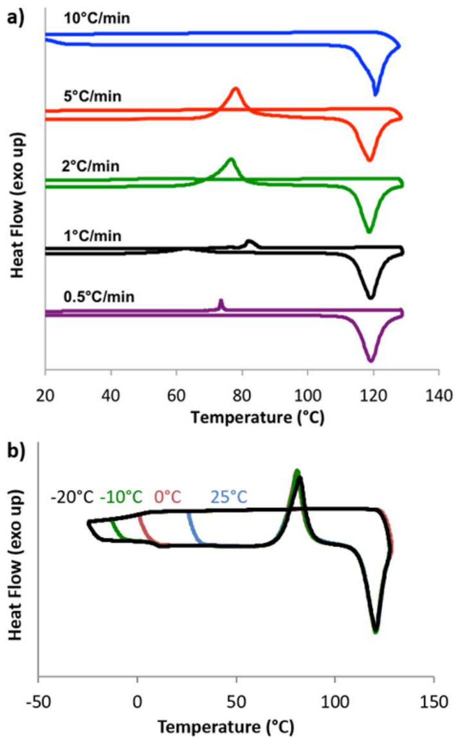

Figure 1. (a) DSC thermograms of consecutive heating/cooling cycles of gbmOMe with varying cooling rates (ramp rate: 10 °C/min). (b) DSC thermograms of gbmOMe cooled to different minimum temperatures (ramp rate: 10 °C/min).

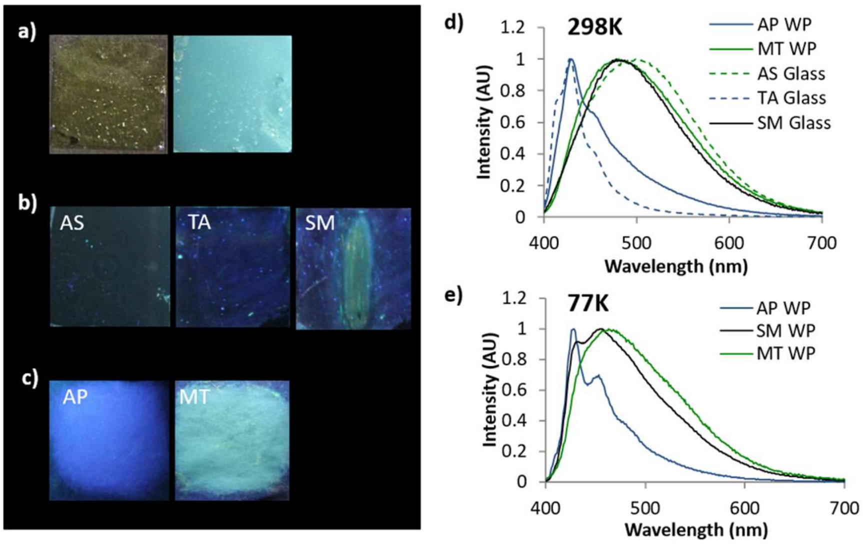

Figure 2. Images of gbmOMe thin films (λ_{ex} = 365 nm) (a) on glass in the melted phase (MT) under ambient (left) and UV light (right) at room temperature; (b) on glass in AS, TA, and SM states at room temperature; and (c) on WP films in AP and MT states. Emission spectra of gbmOMe films (λ_{ex} = 369 nm) on (d) WP and glass at room temperature and (e) WP at 77K.

differences in the cooling rates when samples are quenched (i.e., cooled) in air.

To gain further insight into the identity of the green emissive state, successive DSC scans of gbmOMe were run while varying the minimum cooling temperature from 25 to −20 °C (Figure 1b). When a relatively fast constant rate of heating/cooling (10 °C/min) was used to prevent crystallization of gbmOMe, all scans that were cooled to a sufficiently low temperature showed a glass transition temperature (T_g = 2 °C). Combined with the cooling rate-dependent crystallization, the presence of a clearly defined T_g could indicate a supercooled liquid state for rapidly cooled gbmOMe above T_g that becomes a glass at lower temperatures.

Mechanochromic Luminescence. In addition to thermal responsiveness, changes in solid-state emission of gbmOMe thin films can also be produced mechanically. Thin films of gbmOMe were investigated on both glass (G) and weighing paper (WP) substrates (Figure 2, Table S2). Glass films were fabricated by spin coating dilute (0.018 M) dye/THF solutions on microscope coverslips. In the as spun (AS) state (i.e., after solvent evaporation), gbmOMe films on glass were locked into a transparent state that glowed green (λ_{AS} = 499 nm) under UV light and qualitatively resembled the melt phase. This transparency is atypical given that as spun films are often opaque.[7,21] Typical thermal annealing of BF_2bdk or bdk samples involves heating below the melting temperature followed by cooling to produce a maximally blue-shifted state. However, this process was insufficient to anneal gbmOMe films, which showed no change in emission and remained in the transparent green emissive state after heating and cooling. Instead, gbmOMe films on glass were heated at 75 °C (below T_m = 119 °C) for 10 min, followed by cooling to room temperature, then gentle smearing with a Kimwipe. After ~1 h, blue emissive films formed. To speed up the processing, after smearing, films were again heated at 75 °C for 10 min followed by cooling to produce an opaque, blue emissive, thermally annealed (TA) state (λ_{TA} = 428 nm) (Figure 2d). It is possible that perturbation of the amorphous phase via smearing induced gbmOMe nucleation to form the crystalline TA phase. According to their corresponding XRD pattern, TA thin films on glass were crystalline, and AS films were amorphous (Figure S2). Smearing of TA films produces green emission (λ_{SM} = 478 nm) that self-recovers over the course of a few minutes (Figure 2, Table S2).

Mechanochromic luminescence properties of gbmOMe were also investigated on weighing paper for ready comparison with many previous studies.[21,22] Thin films were prepared by smearing a small amount of gbmOMe (~2 mg) across a piece of weighing paper. The as prepared (AP) WP film glowed blue (λ_{AP} = 428 nm) under UV exposure, and smearing produced green emission that rapidly regained its original blue color (~30 s). Unlike most other ML samples, thermal annealing is not required to produce the maximally blue-shifted state. Recovery happens rapidly and spontaneously. Recovery of smeared WP films was so rapid that an emission spectrum in the SM state could not be obtained at room temperature given that the green smeared emission disappeared faster than the time required to perform the measurement.

The self-healing properties of BF_2bdk ML materials have been previously ascribed by Ito et al., to the thermal back population from the amorphous phase to the crystalline state.[46] In order to slow the rapid recovery of gbmOMe WP films and observe them in the SM state, the optical properties of WP films were measured at 77K (Figure 2e, Table S3). Films in the SM state were produced by rubbing the sample, followed by immediate submersion in liquid N_2. Excitation spectra were also recorded to probe the different emissive species that exist in AP, MT, and SM weigh paper films (Figure S3). The peak emission of smeared films (λ_{SM} = 454 nm) at 77K falls between the slightly red-shifted peak emission of melt films (λ_{MT} = 463 nm) and the blue-shifted peak emission of films in the AP state (λ_{AP} = 429 nm). The relative proximity in peak emission and their similarly broad emission profiles indicate that the smeared and melt states of WP films contain similar emissive species. However, a shoulder corresponding with the emission of AP films is also visible in the spectrum of the smeared film. This suggests that SM gbmOMe samples are comprised of both green amorphous and blue crystalline emissive species. This is further supported by the excitation spectra monitored at the peak emission of each film. The excitation spectrum of the SM sample contains features of AP and SM films. Incomplete conversion of the sample to the amorphous state upon smearing or rapid partial recovery before immersion in liquid nitrogen may explain the presence of blue and green emissive states in the smeared WP film. On the basis of the optical characterization, the mechanically produced color changes observed in gbmOMe films on both glass and WP substrates appear to be produced by the same emissive species.

Structural Characterization. X-ray diffraction studies were performed to gain insight into crystallinity and molecular packing. As previously described, powder XRD patterns of bulk gbmOMe and thermally annealed (TA) glass films indicate that crystalline species produce blue emission and that green emission results from amorphous states (i.e., MT and AS). To further investigate the solid-state emission and intermolecular interactions, single crystals were grown by vapor diffusion of hexanes into a concentrated EtOAc solution of gbmOMe. The emission spectrum of the crystals is similar that of other material forms with blue emissive states; however, the peak emission of the crystal (λ_C = 452 nm) is red-shifted relative to emission of WP films at room temperature (λ_{AP} = 429 nm). The difference in emission profiles could indicate the presence of multiple phases in WP films (Figure S4).

According to the crystal structure, gbmOMe adopts a mostly planar conformation. However, the methoxy group in the 4-position of the trimethoxy substituted phenyl ring is out of plane, which can be attributed to steric crowding by the neighboring methoxy substituents (Figure 3). Despite the presence of a hydroxyl group in gbmOMe, no intermolecular hydrogen bonding is observed. In fact, the only interactions influencing the crystal packing are C−H···O−C, C−H···arene, and weak C−H···H−C van der Waals interactions. For example, multiple C−O···H−Ar interactions (1) between oxygen atoms of meta-(m-OMe) and para- (p-OMe) methoxy groups of the trisubstituted arene ring and aryl hydrogens of an adjacent dye are observed (interaction distances: m-OMe: 2.711 Å, p-OMe: 2.416 Å) Additionally, C−H···O = C interactions (2) are also observed between hydrogen atoms of methoxy groups on the monosubstituted ring and the ketone moiety of neighboring molecules (distance: 2.667 Å) (Figure 3b). Examination of the unit cell shows that gbmOMe molecules are arranged in a herringbone configuration with no evidence of face-to-face or offset dimers often observed for ML active bdk-based materials.[20,47] The intermolecular distance was estimated between neighboring dyes using centroids calculated for the trimethoxy substituted rings of each molecule. As evidenced by the large intermolecular distance (5.334 Å), $\pi-\pi$ interactions were not observed. This may be the result of out-of-plane methoxy substituents in gbmOMe preventing π-stacking and other strong associations linked with dimer formation in similar bdk systems.[48,49] These groups may also play a role in more rapid recovery.

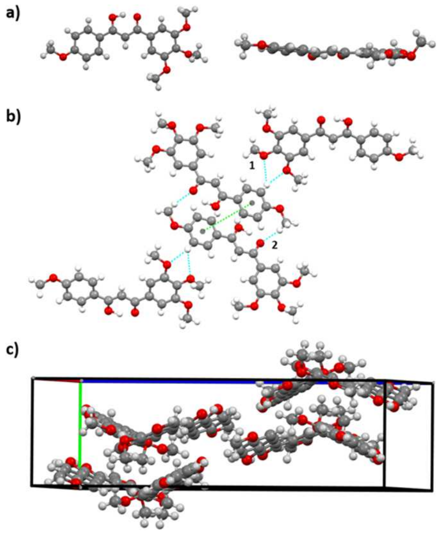

Figure 3. (a) Crystal structure of gbmOMe from top (left) and side (right) view. (b) View highlighting C−O···H−Ar and C−H···O = C interactions in gbmOMe crystals (interaction distances: (1) m-OMe: 2.711 Å; p-OMe: 2.416 Å; (2) 2:2.667 Å) and intermolecular distances (green line; 5.334 Å). (c) Unit cell of gbmOMe.

Camera Characterization of Mechanochromic Luminescence Recovery. The ML behavior of glass and weigh paper films is similar; however, there is a large difference in their recovery times. All samples show blue to green ML, but the smeared emission of WP films vanishes much more quickly compared to that of smeared samples on glass. Film thickness, substrate, or other fabrication effects may be involved. In fact, the rapid recovery of gbmOMe provides a good handle for investigation given the intensity of the SM emission changes on a convenient time scale for measurement.

A camera method was developed to monitor intensity changes during mechanochromic luminescence recovery in gbmOMe films. Specifically, a video was recorded immediately after smearing, and the intensity decay of the smearing induced color changes was monitored for each pixel. The green channel of the camera was used, given significant overlap between its quantum efficiency and the emission profile of the smeared state. Furthermore, the green channel specifically captures the smeared state given that emission from the thermally annealed state does not tail into this region (Figure S5). The smeared-state decay for each pixel (i.e., recovery lifetime, τ_R) was determined using Matlab by fitting the intensity to a double exponential decay and calculating the pre-exponential weighted lifetime (Figures S6 and S7). Using the τ_R for each pixel, a spatially resolved colormap was generated for each video, depicting the smeared region decay process on glass and WP substrates (Figure 4a). By computing the mean τ_R across a region of interest in the colormap, calculation of the average smeared-state lifetime (τ_{SM}) is possible, and processes on WP and glass samples may be compared.

To validate the camera method, it is important to consider other decay pathways that could affect the intensity of emission. For example, continuous UV irradiation for the duration of the video recording could result in photobleaching. To ensure that the photodegradation of gbmOMe does not significantly contribute to the intensity decay, a video of gbmOMe WP films was recorded under constant UV illumination. The intensity change of the green channel was measured for films in AP and MT states given both crystalline and amorphous species are present during the smearing process (Figure 4b). For the photostability control experiment, films were irradiated for over 3 h, which is much longer than gbmOMe recovery on both WP and glass substrates. Films typically recover (i.e., show little change in emission) within seconds (WP) or a few minutes (glass) after smearing. During the course of the 3 h photostability measurement, the intensity of crystalline AP films decreased by ~20%, whereas amorphous MT films showed only a slight decrease in intensity (5−10%) over the

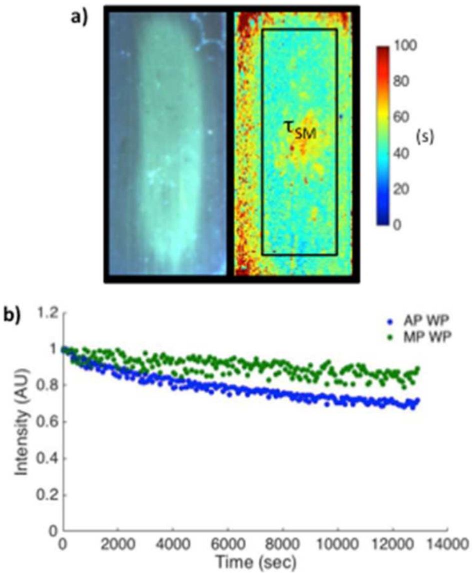

Figure 4. (a) Initial frame from the video of a smeared gbmOMe glass film (left) and the corresponding colormap for the smeared intensity decay process (right). The colormap was generated from the pre-exponential weighted lifetimes of the double exponential fit associated with the intensity decay of the green channel for each pixel (τ_R). A region of interest (black rectangle) was defined to calculate the average lifetime of the smeared state (τ_{SM}). (b) Photostability experiments showing intensity over time of continuously illuminated weigh paper films in the AP and MT states (λ_{ex} = 365 nm).

same time period. Inspection of photostability data for shorter time frames typically used to monitor smeared emission decay (i.e., minutes) revealed that intensity differences were imperceptible. These results indicate that photodegradation is minimal and should not interfere with methods utilizing intensity to calculate smeared emission decay, τ_{SM}.

Sample thickness effects were investigated by three different approaches. Namely, films were prepared by different common methods (i.e., surface application of the solid, drop casting, and spin-casting), by varying the sample loading within a given method (e.g., spin-casting from solutions of different dye concentrations), and by repeated smearing, which removes some sample with each iteration. An initial investigation was conducted to get a rough idea of how these different approaches affect smeared-state decay and to screen for differences. Afterward, a more detailed study was conducted for glass films, and results are presented below.

Films for initial screening were prepared in the following ways. Glass films were prepared by two methods. Thicker glass films were made by drop casting from a concentrated gbmOMe/THF solution (0.090 M) and evaporating in air (G1). Thinner films were produced via spin-casting from the same concentrated (G2) and more dilute (0.018 M) solutions (G3) (note: the fabrication procedure for G3 is the same as that used to make films for ML studies on the glass above). Thicker weigh paper films were fabricated by spreading bulk gbmOMe powder (~2 mg) across the substrate (WP1; standard fabrication procedure for weigh paper ML films above), and thinner films were made by drop casting from the same concentrated (WP2) and dilute (WP3) solutions that were used to produce glass films. Then, glass and WP gbmOMe thin films were repeatedly smeared in the same region, and τ_{SM} was calculated for up to ten smearing/recovery cycles (Figure 5).

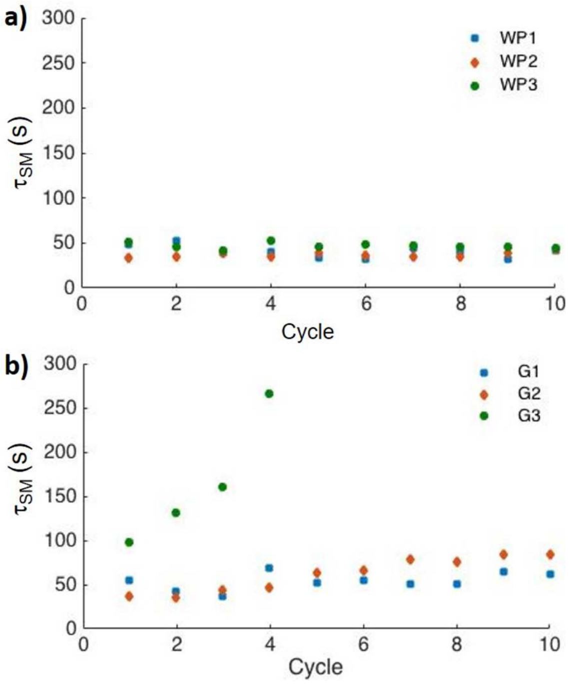

Figure 5. Smeared-state decay (τ_{SM}) of repeatedly smeared gbmOMe thin films on (a) 3″ × 1″ weigh paper and (b) glass substrates (τ_{SM} = smeared-state decay (τ_R, per pixel) averaged over a region of interest).

With the exception of G3, most films show comparable smeared-state decays ($\tau_{SM} < 100$) regardless of substrate and smearing cycle. Data for WP films shows that τ_{SM} fluctuates randomly between 32 and 52 s regardless of the fabrication method (Figure 5a). This fluctuation may simply be due to the noise that can be expected in the fabrication and smearing process. To assess this, the τ_{SM} values for all WP samples were averaged ($\overline{\tau}_{SM}$ = 41.2 s), and the standard deviation was computed to be σ_{SM} = 6.0 s. Comparison of τ_{SM} data for G1 and G2 reveals similar smeared-state decays though G2 and in particular shows a slight upward trend with each smearing cycle (G1: cycle 1 = 55 s; cycle 10 = 68 s; G2: cycle 1 = 36 s; cycle 10 = 84 s) (Figure 5b). For G3, however, the thinnest glass film, this effect is much more dramatic. After the first cycle, τ_{SM} is already roughly double that of G1 and G2 (e.g., G3 τ_{SM} = 98 s; G1 τ_{SM} = 55 s) and increases significantly with each smearing (i.e., thinning) cycle. After the fourth cycle (τ_{SM} = 266 s), the signal intensity was too low for reliable camera detection, so data were no longer recorded. These results point to a film thickness effect upon smeared-state decay and a possible threshold, below which larger decay times are detected. While τ_{SM} represents an average for an entire 2D region of interest, greater resolution is achieved with colormaps, which display smeared-state decays on a pixel-level scale (τ_R). Colormaps associated with both weigh paper (Figure S8) and glass films (Figure S9) show that regions with longer lifetimes are more prevalent in films that are thinner (i.e., initially, upon repeated smearing or due to localized smearing effects at the center of the sample).

Differences between weigh paper and glass samples may arise from substrate or thickness effects, initially or upon repeated smearing. Though G1 and WP2 were drop cast from the same initial solution, cycle 10 smeared-state lifetimes are slightly longer on glass (τ_{SM} = 68 s) than weigh paper (τ_{SM} = 48 s). Furthermore, the colormap of G1 after the tenth cycle shows well-defined regions with large τ_R that are not present in colormaps corresponding to WP2. These findings indicate that the dye likely interacts with cellulose paper fibers differently than with SiO_2 glass. Furthermore, qualitative observations suggest that more sample is removed from hard glass surfaces than from paper with each smearing cycle; additionally, smearing on paper may cause the dye to penetrate into the fibers and be somewhat more resistant to removal with mechanical perturbation. These substrate differences may help to explain why films on paper retain their reversible quality for longer despite similar preparation and treatment as films on glass.

To test whether weigh paper films also reach a point at which τ_{SM} values begin to increase, WP films with initial thicknesses smaller than those of WP1−WP3 were fabricated by spin-casting from a 0.018 M solution. Though spin-casting is somewhat unconventional for paper substrates, it nonetheless addressed challenges associated with drop casting dilute dye solutions, which still produced relatively thick films after evaporation due to the amount of solvent needed to cover the entire sample. After spin-casting and annealing at 75 °C, heterogeneous films were obtained that were thin at the centers and thicker at the edges, as confirmed by colormap histograms with bimodal distributions (Figure S10). Though a thickness gradient was observed, these films allow monitoring of the distribution of smeared-state decays on the same surface. After the first smearing/recovery cycle, the colormap showed regions with longer recovery lifetimes (τ_R) where the sample was thinnest compared to the thicker edges that recovered more quickly (Figure 6). The colormaps for subsequent smearing/recovery cycles show the erosion of the thicker regions of the sample and a general trend toward longer smeared-state decays. Furthermore, the smeared-state decays (i.e., calculated from recovery lifetimes τ_R for a region of interest that encompasses both thicker and thinner regions) for each of the cycles (τ_{SM} = 66 s for cycle 1; τ_{SM} = 79 s for cycle 2; τ_{SM} = 83 s for cycle 3) were significantly longer than those observed for bulk and drop cast WP1−WP3 films ($35 < \tau_{SM} < 55$ s). Not only does this clearly demonstrate thickness-dependent recovery on weigh paper substrates, it also shows that differences in ML recovery behavior can be used to evaluate relative film thickness in a given heterogeneous sample.

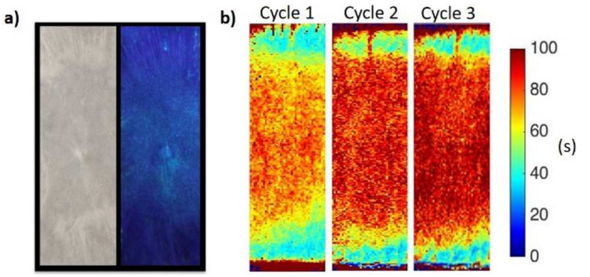

Figure 6. (a) Images of spin-cast gbmOMe films on WP under ambient light (left) and UV irradiation (right). (b) Spatially resolved colormaps of repeatedly smeared spin-cast gbmOMe on WP (λ_{ex} = 365 nm).

According to the initial studies, it is clear that the recovery dynamics of gbmOMe thin films are dependent on sample thickness. Smeared-state decays increase with decreasing film thickness, and quite dramatically so for the thinnest samples. To investigate these effects more systematically using a single common film fabrication method and substrate, gbmOMe thin films of variable thickness were prepared via spin-casting from stock solutions of different concentrations (C1 = 0.090 M; C2 = 0.072 M; C3 = 0.054 M; C4 = 0.036 M; C5 = 0.018 M) on glass. This range is bracketed by concentrations used to fabricate G1 and G3 films above. Multiple films were prepared from each solvent, and the relative film thickness was estimated by measuring the absorption spectrum of each film in the AS state and using the peak absorption (λ_{abs} = 363 nm) and Beer's Law to calculate the corresponding path length of each film (Figure S11). Films in the AS state were used to determine relative initial thickness due to their transparency; TA films are opaque and incompatible with this measurement method given scattering effects. Approximate thicknesses were calculated relative to the thinnest film such that the maximum thickness was over eight times greater in the initial AS state. On the basis of the absorption spectra, some deviations in thickness were observed when spin-casting from stock solutions of the same concentration. This was especially evident for films fabricated from solution C1. Samples spin-cast from concentrated solutions produce less reproducible film thicknesses, which account for multiple points per concentration in Figure 7b. After annealing, each film was smeared in three separate locations with a cotton swab for finer control (Figure 7). Then, τ_{SM} values for each smeared region were averaged to quantify the recovery dynamics for a given film (Figure 7b) (mean τ_{SM} = $\overline{\tau}_{SM}$). This approach provides insight into the reproducibility of smeared-state decay values for regions of comparable thickness.

The representative colormaps for films of different initial thicknesses, T1−T5, produced via spin-casting from different solvents, C1−C5, show a narrow distribution of smeared-state decays within each smeared region (Figure 7). A relatively narrow range of $\overline{\tau}_{SM}$ values (26−41 s) was observed for all but the thinnest samples (max $\overline{\tau}_{SM}$ = 120 s), which corresponds to an 87% decrease in initial thickness compared to the thickest sample. Furthermore, most samples showed very little variation in $\overline{\tau}_{SM}$ regardless of the region being sampled; however, the thinnest samples showed the most significant deviation (e.g., T5, SM1). Despite the relatively large error bars associated with data for the thinnest samples, $\overline{\tau}_{SM}$ was still significantly longer compared to thicker film decays. The trend toward longer $\overline{\tau}_{SM}$ for thinner films is additional evidence of a thickness effect in gbmOMe glass films, and here, too, it appears that a critical thickness threshold must be reached before thickness effects are detected and smeared-state decays noticeably increase.

To gain further insight into a possible thickness threshold, the regime where smeared-state decays change most dramatically, another set of films with varying initial thicknesses, T6−T10, was prepared using the same method as described above. These films were further thinned by repeated smearing for five cycles (Figure 8). As expected, regions of longer smeared-state decay (τ_{SM} > 100 s) developed and grew as the sample was continuously smeared. For thinner samples, these areas became pronounced after fewer cycles. This trend is illustrated by comparing the two extremes. For the thickest sample, T6, red colored regions with elevated recovery lifetimes started to develop only after cycle 4. However, for T10, the thinnest sample, longer recovery lifetimes were observed beginning with the first cycle. Additionally, as T10 was repeatedly smeared, the size of the longer recovering red region increased such that it

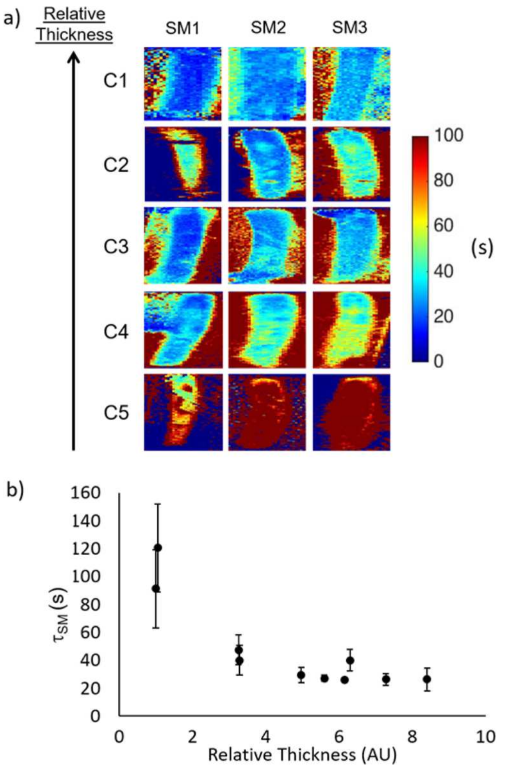

Figure 7. (a) Representative recovery lifetime (τ_R) colormaps of spin-cast gbmOMe thin films on glass with different initial thicknesses fabricated via spin-casting from different concentration stock solutions. Relative thicknesses were calculated from absorption spectra of each film. Three different regions of each film (SM1, SM2, and SM3) were smeared with a cotton swab to assess reproducibility of smeared-state decays without changing initial thickness due to sample removal. Thicknesses T1−T5 represent films spin-cast from progressively more dilute stock solutions (C1 = 0.090 M; C2 = 0.072 M; C3 = 0.054 M; C4 = 0.036 M; C5 = 0.018 M). (b) Mean smeared-state decays ($\overline{\tau}_{SM}$) as a function of relative thickness. Error bars represent one standard deviation from the mean $\overline{\tau}_{SM}$ for each sample and indicate smearing and thickness variations within a given film. Multiple films were made from each stock solution, which produced films with slight variations in initial thicknesses.

encompassed nearly the entire film after the third recovery cycle. After five smearing cycles, larger τ_{SM} values were observed for all samples regardless of initial film thickness; however, the increases in τ_{SM} are less significant for the thickest sample. One potential explanation for this deviation is that the thickness of T6 has not yet reached a critical region even after five smearing/recovery cycles. As observed for the first cycle, a general upward trend was observed with decreasing initial thickness until a maximum smeared-state decay (τ_{SM} = 104 s) was measured for T10. Coupled with the results for the colormaps, these trends in τ_{SM} provide further evidence that the smeared-state decay is highly dependent on the film thickness of gbmOMe.

Experiments indicate that τ_{SM} is relatively insensitive to thickness effects until a critical threshold is reached. This is evidenced by the small deviations in τ_{SM} that were observed until a requisite amount of gbmOMe was removed, and films with smaller initial thicknesses show longer τ_{SM} values (Figure 9). One potential explanation for this apparent thickness threshold is that sample−substrate interactions become more significant for thinner films and slow ML recovery. Thus, a certain amount of sample must be removed from thicker films before accessing an interfacial regime where substrate interactions can be observed. It is also possible that the material morphology changes in thinner films. Given that ML is a solid-state property, a certain particle size and number and arrangement of molecules is likely required in the extended array to observe rapid reversibility. The thinnest of samples explored in this study may reach the limits of this regime for gbmOMe.

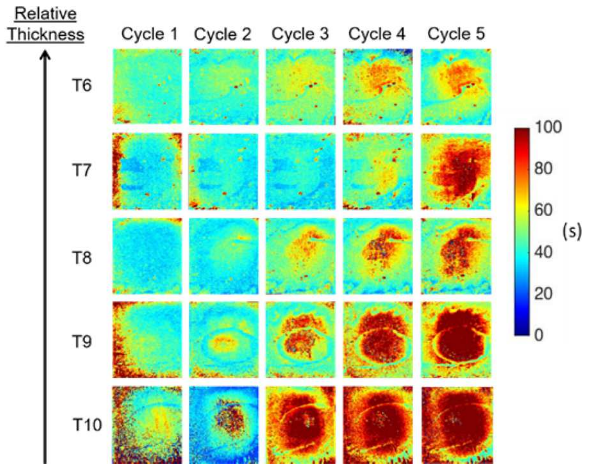

Figure 8. Spatially resolved smeared-state decay colormaps of repeatedly smeared spin-cast gbmOMe thin films with varying thicknesses on glass substrates. Samples were smeared with a Kimwipe for 2 s to aim for consistent sample removal for 5 smearing/recovery cycles. T6−T10 represent films spin-cast from progressively more dilute stock solutions (T6 = 0.090 M; T7 = 0.072 M; T8 = 0.054 M; T9 = 0.036 M; T10 = 0.014 M).

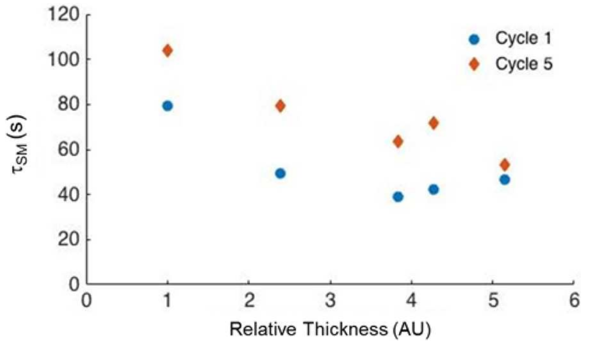

Figure 9. Smeared-state decay (τ_{SM}) versus relative initial thickness of smeared gbmOMe glass films after one and five smearing/recovery cycles.

■ CONCLUSION

Stimuli responsive gbmOMe has many interesting thermal and mechanochromic properties. As a thin film, gbmOMe forms a thermally stable supercooled liquid phase when melted and subsequently cooled at ambient temperature. Yet, when the bulk dye is cooled at room temperature, a metastable supercooled liquid state is formed, which eventually recrystallizes after a few minutes. Mechanochromic properties include a blue to green shift in emission upon smearing along with rapid ML recovery at room temperature. This presents a unique handle for evaluating the performance of self-recovering ML materials by a new camera method. The intensity decay of each pixel (i.e., recovery lifetime, τ_R) was used to generate a spatially resolved colormap of the recovery process. When averaged over a region of interest, smeared-state decay values τ_{SM} were calculated and provided a means of comparison between different sample preparations, substrates, and film thicknesses. Findings with thicker films illustrate the potential of gbmOMe as a dynamic "renewable ink" with the ability to recover even after repeated use. Thin films of gbmOMe, however, showed thickness-dependent smeared-state decays on both glass and WP substrates, but significant fluctuations in recovery behavior were observed only in the thinnest films investigated, indicating that a critical thickness must be reached before gbmOMe films lose full reversibility. Kim et al. showed that quantitative force measurements yield reliable results for uniform films but are unreliable for molecular solids with heterogeneous coverage.[36] These results show, however, that smeared-state decays obtained from camera analysis are quite reproducible even with a qualitative smearing method. Particularly for fast recovering ML systems, films of similar thickness on identical substrates must be used to accurately compare and quantify recovery in ML materials. Additionally, threshold effects may well vary for different reversible ML dyes and substrates and should be identified in each case. Future studies with functionalized surfaces may provide additional insight into the origin of substrate effects and new methods for modulating ML recovery. For certain applications, it may be desirable to generate films that can fully recover after many smearing/self-erasing cycles. Methods that greatly hinder or prevent sample removal and a reduction in sample thickness would be important. Other dye−substrate combinations and protective coatings that do not significantly affect ML color change and recovery behaviors are avenues worth exploring.

■ ASSOCIATED CONTENT

Ⓢ Supporting Information

The Supporting Information is available free of charge on the ACS Publications website at DOI: 10.1021/acsami.7b01985.

Spectra and data tables for gbmOMe glass and WP films at room temperature and 77 K, X-ray diffraction patterns for the different phases of gbmOMe, additional experimental details for the camera detection method, colormaps for repeatedly smeared glass and WP thin films, absorbance spectra of spin-cast glass films from different concentration gbmOMe/THF stock solutions, and colormaps and histograms of smeared-state decays of repeatedly smeared WP films fabricated via spin-casting (PDF)

Mechanochromic luminescence recovery processes for gbmOMe films AP on weigh paper (AVI)

Mechanochromic luminescence recovery processes for gbmOMe films spin-cast on weigh paper (AVI)

Mechanochromic luminescence recovery processes for gbmOMe films spin-cast on glass (AVI)

(CIF)

■ AUTHOR INFORMATION

Corresponding Author

*E-mail: fraser@virginia.edu.

ORCID

Cassandra L. Fraser: 0000-0002-8927-4694

Notes

The authors declare no competing financial interest.

■ ACKNOWLEDGMENTS

We thank the National Science Foundation (NSF Grant CHE-1213915) and the University of Virginia Department of Chemistry for support for this research and Professor James Demas for helpful discussions concerning the camera detection method.

■ REFERENCES

(1) Morris, W. A.; Kolpaczynska, M.; Fraser, C. L. Effects of α-Substitution on Mechanochromic Luminescence and Aggregation-Induced Emission of Difluoroboron β- Diketonate Dyes. *J. Phys. Chem. C* **2016**, *120*, 22539−22548.

(2) Zhang, G.; Lu, J.; Fraser, C. L. Mechanochromic Luminescence Quenching: Force-Enhanced Singlet-to-Triplet Intersystem Crossing for Iodide-Substituted Difluoroboron−Dibenzoylmethane−Dodecane in the Solid State. *Inorg. Chem.* **2010**, *49*, 10747−10749.

(3) Zhang, G.; Lu, J.; Sabat, M.; Fraser, C. L. Polymorphism and Reversible Mechanochromic Luminescence for Solid-State Difluoroboron Avobenzone. *J. Am. Chem. Soc.* **2010**, *132*, 2160−2162.

(4) Zhang, G.; Palmer, G. M.; Dewhirst, M. W.; Fraser, C. L. A Dual-Emissive-Materials Design Concept Enables Tumour Hypoxia Imaging. *Nat. Mater.* **2009**, *8*, 747−751.

(5) DeRosa, C. A.; Samonina-Kosicka, J.; Fan, Z.; Hendargo, H. C.; Weitzel, D. H.; Palmer, G. M.; Fraser, C. L. Oxygen Sensing Difluoroboron Dinaphthoylmethane Polylactide. *Macromolecules* **2015**, *48*, 2967−2977.

(6) DeRosa, C. A.; Seaman, S. A.; Mathew, A. S.; Gorick, C. A.; Fan, Z.; Demas, J. N.; Peirce, S. M.; Fraser, C. L. Oxygen Sensing Difluoroboron β−Diketonate Polylactide Materials with Tunable Dynamic Ranges for Wound Imaging. *ACS Sens.* **2016**, *1*, 1366−1373.

(7) Nguyen, N. D.; Zhang, G.; Lu, J.; Sherman, A. E.; Fraser, C. L. Alkyl Chain Length Effects on Solid-State Difluoroboron β-Diketonate Mechanochromic Luminescence. *J. Mater. Chem.* **2011**, *21*, 8409−8415.

(8) Zhang, X.; Liu, X.; Lu, R.; Zhang, H.; Gong, P. Fast Detection of Organic Amine Vapors Based on Fluorescent Nanofibrils Fabricated from Triphenylamine Functionalized β-Diketone-Boron Difluoride. *J. Mater. Chem.* **2012**, *22*, 1167−1172.

(9) Zhang, G.; Kim, S. H.; Evans, R. E.; Kim, B. H.; Demas, J. N.; Fraser, C. L. Luminescent Donor-Acceptor β-Diketones: Modulation of Emission by Solvent Polarity and Group II Metal Binding. *J. Fluoresc.* **2009**, *19*, 881−889.

(10) Zeng, S.; Zhang, D.; Huang, W.; Wang, Z.; Freire, S. G.; Yu, X.; Smith, A. T.; Huang, E. Y.; Nguon, H.; Sun, L. Bio-Inspired Sensitive and Reversible Mechanochromisms via Strain-Dependent Cracks and Folds. *Nat. Commun.* **2016**, *7*, 11802.

(11) Ciardelli, F.; Ruggeri, G.; Pucci, A. Dye-Containing Polymers: Methods for Preparation of Mechanochromic Materials. *Chem. Soc. Rev.* **2013**, *42*, 857−870.

(12) Sagara, Y.; Yamane, S.; Mitani, M.; Weder, C.; Kato, T. Mechanoresponsive Luminescent Molecular Assemblies: An Emerging Class of Materials. *Adv. Mater.* **2016**, *28*, 1073−1095.

(13) Chi, Z.; Zhang, X.; Xu, B.; Zhou, X.; Ma, C.; Zhang, Y.; Liu, S.; Xu, J. Recent Advances in Organic Mechanofluorochromic Materials. *Chem. Soc. Rev.* **2012**, *41*, 3878−3896.

(14) Zhang, X.; Chi, Z.; Zhang, Y.; Liu, S.; Xu, J. Recent Advances in Mechanochromic Luminescent Metal Complexes. *J. Mater. Chem. C* **2013**, *1*, 3376−3390.

(15) Fang, Y.; Ni, Y.; Leo, S.-Y.; Wang, B.; Basile, V.; Taylor, C.; Jiang, P. Direct Writing of Three-Dimensional Macroporous Photonic Crystals on Pressure-Responsive Shape Memory Polymers. *ACS Appl. Mater. Interfaces* **2015**, *7*, 23650−23659.

(16) Jiang, Y. An Outlook Review: Mechanochromic Materials and Their Potential for Biological and Healthcare Applications. *Mater. Sci. Eng., C* **2014**, *45*, 682−689.

(17) Butler, T.; Morris, W. A.; Samonina-Kosicka, J.; Fraser, C. L. Mechanochromic Luminescence and Aggregation Induced Emission for a Metal-Free β-Diketone. *Chem. Commun.* **2015**, *51*, 3359−3362.

(18) Butler, T.; Morris, W. A.; Samonina-Kosicka, J.; Fraser, C. L. Mechanochromic Luminescence and Aggregation Induced Emission of Dinaphthoylmethane β-Diketones and Their Boronated Counterparts. *ACS Appl. Mater. Interfaces* **2016**, *8*, 1242−1251.

(19) Hubaud, J. C.; Bombarda, I.; Decome, L.; Wallet, J. C.; Gaydou, E. M. Synthesis and Spectroscopic Examination of Various Substituted 1,3-Dibenzoylmethane, Active Agents for UVA/UVB Photoprotection. *J. Photochem. Photobiol., B* **2008**, *92*, 103−109.

(20) Morris, W. A.; Sabat, M.; Butler, T.; DeRosa, C. A.; Fraser, C. L. Modulating Mechanochromic Luminescence Quenching of Alkylated Iodo Difluoroboron Dibenzoylmethane Materials. *J. Phys. Chem. C* **2016**, *120*, 14289−14300.

(21) Morris, W. A.; Liu, T.; Fraser, C. L. Mechanochromic Luminescence of Halide-Substituted Difluoroboron β-Diketonate Dyes. *J. Mater. Chem. C* **2015**, *3*, 352−363.

(22) Liu, T.; Chien, A. D.; Lu, J.; Zhang, G.; Fraser, C. L. Arene Effects on Difluoroboron β-Diketonate Mechanochromic Luminescence. *J. Mater. Chem.* **2011**, *21*, 8401−8408.

(23) Shen, X. Y.; Yuan, W. Z.; Liu, Y.; Zhao, Q.; Lu, P.; Ma, Y.; Williams, I. D.; Qin, A.; Sun, J. Z.; Tang, B. Z. Fumaronitrile-Based Fluorogen: Red to Near-Infrared Fluorescence, Aggregation-Induced Emission, Solvatochromism, and Twisted Intramolecular Charge Transfer. *J. Phys. Chem. C* **2012**, *116*, 10541−10547.

(24) Han, T.; Gu, X.; Lam, J. W. Y.; Leung, A. C. S.; Kwok, R. T. K.; Han, T.; Tong, B.; Shi, J.; Dong, Y.; Tang, B. Z. Diaminomaleonitrile-Based Schiff Bases: Aggregation-Enhanced Emission, Red Fluorescence, Mechanochromism and Bioimaging Applications. *J. Mater. Chem. C* **2016**, *4*, 10430−10434.

(25) Poon, C.-T.; Wu, D.; Lam, W. H.; Yam, V. W. A Solution-Processable Donor-Acceptor Compound Containing Boron(III) Centers for Smal0l-Molecule-Based High-Performance Ternary Electronic Memory Devices. *Angew. Chem.* **2015**, *127*, 10715−10719.

(26) Gong, Y.; Tan, Y.; Liu, J.; Lu, P.; Feng, C.; Yuan, W. Z.; Lu, Y.; Sun, J. Z.; He, G.; Zhang, Y. Twisted D-π-A Solid Emitters: Efficient Emission and High Contrast Mechanochromism. *Chem. Commun.* **2013**, *49*, 4009−4011.

(27) Mutai, T.; Satou, H.; Araki, K. Reproducible On−off Switching of Solid-State Luminescence by Controlling Molecular Packing through Heat-Mode Interconversion. *Nat. Mater.* **2005**, *4*, 685−687.

(28) Liu, W.; Wang, Y.; Sun, M.; Zhang, D.; Zheng, M.; Yang, W. Alkoxy-Position Effects on Piezofluorochromism and Aggregation-Induced Emission of 9,10-Bis(alkoxystyryl)anthracenes. *Chem. Commun.* **2013**, *49*, 6042−6044.

(29) Zhang, X.; Ma, Z.; Yang, Y.; Zhang, X.; Jia, X.; Wei, Y. Fine-Tuning the Mechanofluorochromic Properties of Benzothiadiazole-Cored Cyano-Substituted Diphenylethene Derivatives through D−A Effect. *J. Mater. Chem. C* **2014**, *2*, 8932−8938.

(30) Zhang, X.; Chi, Z.; Xu, B.; Jiang, L.; Zhou, X.; Zhang, Y.; Liu, S.; Xu, J. Multifunctional Organic Fluorescent Materials Derived from 9,10-Distyrylanthracene with Alkoxyl Endgroups of Various Lengths. *Chem. Commun.* **2012**, *48*, 10895−10897.

(31) Galer, P.; Korošec, R. C.; Vidmar, M.; Šket, B. Crystal Structures and Emission Properties of the BF_2 Complex 1-Phenyl-3-(3,5-Dimethoxyphenyl)-Propane-1,3-Dione: Multiple Chromisms, Aggregation- or Crystallization-Induced Emission, and the Self-Assembly Effect. *J. Am. Chem. Soc.* **2014**, *136*, 7383−7394.

(32) Samonina-Kosicka, J.; Derosa, C. A.; Morris, W. A.; Fan, Z.; Fraser, C. L. Dual-Emissive Difluoroboron Naphthyl-Phenyl β-Diketonate Polylactide Materials: Effects of Heavy Atom Placement and Polymer Molecular Weight. *Macromolecules* **2014**, *47*, 3736−3746.

(33) Hariharan, P. S.; Venkataramanan, N. S.; Moon, D.; Anthony, S. P. Self-Reversible Mechanochromism and Thermochromism of a Triphenylamine-Based Molecule: Tunable Fluorescence and Nanofabrication Studies. *J. Phys. Chem. C* **2015**, *119*, 9460−9469.

(34) Morris, W. A.; Butler, T.; Kolpaczynska, M.; Fraser, C. L. Stimuli Responsive Furan and Thiophene Substituted Difluoroboron β-Diketonate Materials. *Mater. Chem. Front.* **2017**, *1*, 158−166.

(35) Mizuguchi, K.; Kageyama, H.; Nakano, H. Mechanochromic Luminescence of 4-[bis(4-Methylphenyl)amino]benzaldehyde. *Mater. Lett.* **2011**, *65*, 2658−2661.

(36) Chung, K.; Kwon, M. S.; Leung, B. M.; Wong-Foy, A. G.; Kim, M. S.; Kim, J.; Takayama, S.; Gierschner, J.; Matzger, A. J.; Kim, J. Shear-Triggered Crystallization and Light Emission of a Thermally Stable Organic Supercooled Liquid. *ACS Cent. Sci.* **2015**, *1*, 94−102.

(37) Shirota, Y.; Kageyama, H. Charge Carrier Transporting Molecular Materials and Their Applications in Devices. *Chem. Rev.* **2007**, *107*, 953−1010.

(38) Shirota, Y. Photo- and Electroactive Amorphous Molecular Materials-Molecular Design, Syntheses, Reactions, Properties, and Applications. *J. Mater. Chem.* **2005**, *15*, 75−93.

(39) Zografi, G.; Newman, A. Interrelationships Between Structure and the Properties of Amorphous Solids of Pharmaceutical Interest. *J. Pharm. Sci.* **2017**, *106*, 5−27.

(40) Mathew, A. S.; De Rosa, C. A.; Demas, J. N.; Fraser, C. L.; DeRosa, C. A.; Demas, J. N.; Fraser, C. L. Difluoroboron β-Diketonate Materials with Long-Lived Phosphorescence Enable Lifetime Based Oxygen Imaging with a Portable Cost Effective Camera. *Anal. Methods* **2016**, *8*, 3109−3114.

(41) Williams, D. B. G.; Lawton, M. Drying of Organic Solvents: Quantitative Evaluation of the Efficiency of Several Desiccants. *J. Org. Chem.* **2010**, *75*, 8351−8354.

(42) Carraway, E. R.; Demas, J. N.; DeGraff, B. A. Luminescence Quenching Mechanism for Microheterogeneous Systems. *Anal. Chem.* **1991**, *63*, 332−336.

(43) Zhu, H.; Wang, X.; Li, Y.; Wang, Z.; Yang, F.; Yang, X. Microwave Synthesis of Fluorescent Carbon Nanoparticles with Electrochemiluminescence Properties. *Chem. Commun.* **2009**, 5118−5120.

(44) Chow, Y. L.; Johansson, C. I.; Zhang, Y.-H.; Gautron, R.; Yang, L.; Rassat, A.; Yang, S.-Z. Spectroscopic and Electrochemical Properties of 1,3-Diketonatoboron Derivatives. *J. Phys. Org. Chem.* **1996**, *9*, 7−16.

(45) Heller, C. A.; Henry, R. A.; McLaughlin, B. A.; Bliss, D. E. Fluorescence Spectra and Quantum Yields. Quinine, Uranine, 9,10-Diphenylanthracene, and 9,10-Bis(phenylethynyl)anthracenes. *J. Chem. Eng. Data* **1974**, *19*, 214−219.

(46) Ito, F.; Sagawa, T. Quantitative Evaluation of Thermodynamic Parameters for Thermal Back-Reaction after Mechanically Induced Fluorescence Change. *RSC Adv.* **2013**, *3*, 19785−19788.

(47) Sun, X.; Zhang, X.; Li, X.; Liu, S.; Zhang, G. A Mechanistic Investigation of Mechanochromic Luminescent Organoboron Materials. *J. Mater. Chem.* **2012**, *22*, 17332−17339.

(48) Morris, W. A.; Sabat, M.; Butler, T.; DeRosa, C. A.; Fraser, C. L. Modulating Mechanochromic Luminescence Quenching of Alkylated Iodo Difluoroboron Dibenzoylmethane Materials. *J. Phys. Chem. C* **2016**, *120*, 14289−14300.

(49) Fedorenko, E. V.; Mirochnik, A. G.; Beloliptsev, A. Y.; Isakov, V. V. (S2→S0) and (S1→S0) Luminescence of Dimethylaminostyryl-β-Diketonates of Boron Difluoride. *Dyes Pigm.* **2014**, *109*, 181−188.